Spectral line commissioning NE54 narrowband mode – L-band

Michael Rugel, Arshia Jacob, Andreas Brunthaler, Friedrich Wyrowski,
Sarwar Khan, Karl Menten (for the MMGPS spectral line/imaging team)

February 24, 2023

Objectives: We present commissioning observations to test the capabilities of the narrowband mode in view of upcoming S- and L-band observations at high spectral resolution. The goal of this commissioning was to observe ∼ 20 star-forming regions in order to obtain the ground state hyperfine-structure splitting transitions of methylidyne (CH) near 3.3 GHz and hydroxyl (OH) at 1.6 GHz alongside the HI 21 cm transition to complement the far-infrared dataset collected as a part of the SOFIA Legacy program HyGAL (Jacob et al. 2022). This commissioning report addresses L-band observations.
The particular focus of these commissioning observations was to verify the ability of the new NE54 narrowband mode to measure spectrally narrow maser emission, as well as to test the setup of the instrument towards lines of interest, as typical OH masers can be narrower than the 0.3 km/s width provided by the NE54 narrowband mode. We would like to address the following questions:

- Can the flux of narrow lines be recovered, which are unresolved at the spectral resolution of the system?
- Is there a flux dependence on the tuning frequency of the band?
- Are the chosen tunings adequate for spectral line observations at L-band?

We observed the HI 21 cm line and three of the four OH hyperfine-structure splitting lines in four different setups (Table 1). The observations were split into two long observations of 10 minutes per source with tunings of the NE54 at 1666 and 1667 MHz, as well as two shorter observations of 5 minutes at 1420 and 1612 MHz. We compared these to ancillary observations carried out with the JVLA (Busch et al. in prep; Rugel et al., in prep; priv. comm.). We observed four sources, NGC6334 I, G09.622+0.19, W49N and W51, which were selected for emission strength of the OH masers. We note that some of the maser components may be variable (e.g., MacLeod et al. 2018; Goedhart et al. 2019).

Observations and data reduction: We tested the narrowband correlator mode NE54 in L-band with 32k channels, which covers a 54 MHz bandwidth of which the inner ∼50 % are usable with a native channel width of 1.633 kHz (∼0.3 km s^{-1}at 1.7 GHz). The observations were conducted on May 26/27, 2022.

We chose four different tunings at 1420 MHz (Table 1; NE54-1420), 1612 MHz (NE54-1612), and 1666 MHz (NE54-1666) and 1667 MHz (NE54-1667) to observe the HI, OH 1612 MHz and the two OH 1665 and 1667 MHz transitions. The OH "main lines" at 1665 and 1667 MHz were captured in both the NE54-1666 and NE54-1667 tunings. Reason was that for a subset of the sources, this shift in central frequency meant that the

Table 1: Hydrogen and hydroxyl hyperfine-splitting transitions observed in four different tunings of the NE54 mode.

Transition $F' - F''$	Frequency [MHz]	Narrowband setup
H 1 – 0	1420.40580	NE54-1420
OH $1^+ - 2^-$	1612.231	NE54-1612
OH $1^+ - 1^-$	1665.402	NE54-1666 & NE54-1667
OH $2^+ - 2^-$	1667.359	NE54-1666 & NE54-1667
OH $2^+ - 1^-$	1720.530	not covered by MeerKAT

Table 2: Comparison of MeerKAT observations of the OH 1665 and 1667 MHz transitions in different tunings.

Source							Transition	NE54-1666 MHz		NE54-1667 MHz		
	R.A.	Dec	l	b	v_{min}	v_{max}		Beam	S_{int}	Beam	S_{int}	Diff
	[h:m:s]	[d:m:s]	[deg]	[deg]	[km/s]	[km/s]		[arcsec]	[Jy/b km/s]	[arcsec]	[Jy/b km/s]	[%]
G09.622+0.19	18:06:14.6864	-20:31:32	9.621	0.196	0.0	3.0	OH 1665 MHz	$10\farcs3 \times 7\farcs2$	27.29	$9\farcs9 \times 6\farcs3$	26.94	-1.25
G09.622+0.19	18:06:14.6864	-20:31:32	9.621	0.196	0.0	3.1	OH 1667 MHz	$10\farcs3 \times 7\farcs1$	25.35	$9\farcs9 \times 6\farcs3$	25.46	0.44
NGC6334 I	17:20:53.35	-35:47:01.5	351.417	0.645	-9.8	-8.1	OH 1665 MHz	$10\farcs5 \times 6\farcs2$	320.91	$9\farcs9 \times 5\farcs9$	322.54	0.51
NGC6334 I	17:20:53.35	-35:47:01.5	351.417	0.645	-12.2	-8.7	OH 1667 MHz	$10\farcs4 \times 6\farcs2$	76.38	$9\farcs9 \times 5\farcs9$	80.81	5.80
W49N	19:10:13.2	+09:06:13	43.166	0.012	14.0	22.0	OH 1665 MHz	$14\farcs7 \times 9\farcs6$	451.69	$11\farcs4 \times 8\farcs1$	453.28	0.35
W49N	19:10:13.4701	+09:06:14	43.167	0.011	4.8	5.5	OH 1667 MHz	$14\farcs7 \times 9\farcs6$	49.23	$11\farcs4 \times 8\farcs1$	45.56	-7.45
W51	19:23:43.9	+14:30:34	49.490	-0.388	54.5	56.6	OH 1665 MHz	$17\farcs6 \times 9\farcs0$	41.87	$12\farcs7 \times 7\farcs8$	40.81	-2.53
W51	19:23:43.9689	+14:30:28	49.488	-0.389	60.5	63.3	OH 1667 MHz	$17\farcs6 \times 9\farcs0$	12.34	$12\farcs7 \times 7\farcs8$	12.49	1.22

Table 3: Comparison of MeerKAT and JVLA observations of the OH 1665 and 1667 MHz transitions.

Source							Transition	NE54-1666 MHz		VLA		
	R.A.	Dec	l	b	v_{min}	v_{max}		Beam	S_{int}	Beam	S_{int}	Diff
	[h:m:s]	[d:m:s]	[deg]	[deg]	[km/s]	[km/s]		[arcsec]	[Jy/b km/s]	[arcsec]	[Jy/b km/s]	[%]
G09.622+0.19	18:06:14.6864	-20:31:32	9.621	0.196	0.0	3.0	OH 1665 MHz	$10\farcs3 \times 7\farcs2$	27.29	$20\farcs3 \times 10\farcs9$	24.56	-9.98
G09.622+0.19	18:06:14.6864	-20:31:32	9.621	0.196	0.0	3.1	OH 1667 MHz	$10\farcs3 \times 7\farcs1$	25.35	$20\farcs3 \times 10\farcs9$	22.35	-11.85
NGC6334 I	17:20:53.35	-35:47:01.5	351.417	0.645	-9.8	-8.1	OH 1665 MHz	$10\farcs5 \times 6\farcs2$	320.91	$28\farcs9 \times 10\farcs4$	283.92	-11.52
NGC6334 I	17:20:53.35	-35:47:01.5	351.417	0.645	-12.2	-8.7	OH 1667 MHz	$10\farcs4 \times 6\farcs2$	76.38	$28\farcs8 \times 10\farcs4$	72.64	-4.89
W49N	19:10:13.2	+09:06:13	43.166	0.012	14.0	22.0	OH 1665 MHz	$14\farcs7 \times 9\farcs6$	451.69	$14\farcs3 \times 11\farcs6$	463.24	2.56
W49N	19:10:13.4701	+09:06:14	43.167	0.011	4.8	5.5	OH 1667 MHz	$14\farcs7 \times 9\farcs6$	49.23	$14\farcs2 \times 10\farcs8$	49.98	1.52
W51	19:23:43.9	+14:30:34	49.490	-0.388	54.5	56.6	OH 1665 MHz	$17\farcs6 \times 9\farcs0$	41.87	$13\farcs8 \times 11\farcs0$	42.59	1.70
W51	19:23:43.9689	+14:30:28	49.488	-0.389	60.5	63.3	OH 1667 MHz	$17\farcs6 \times 9\farcs0$	12.34	$14\farcs7 \times 11\farcs2$	12.06	-2.24

Table 4: Comparison of MeerKAT and JVLA observations of the OH 1612 MHz transition.

Source							NE54-1612 MHz		VLA		
	R.A.	Dec	l	b	v_{min}	v_{max}	Beam	S_{int}	Beam	S_{int}	Diff
	[h:m:s]	[d:m:s]	[deg]	[deg]	[km/s]	[km/s]	[arcsec]	[Jy/b km/s]	[arcsec]	[Jy/b km/s]	[%]
G09.622+0.19	18:06:13.9034	-20:31:46.9998	9.616	0.196	0.0	3.0	$35\farcs0 \times 35\farcs0$	1.02	$35\farcs0 \times 35\farcs0$	1.07	4.73
NGC6334 I	17:20:53.5144	-35:47:03.5	351.417	0.644	-8.7	-6.2	$35\farcs0 \times 35\farcs0$	2.87	$35\farcs0 \times 35\farcs0$	0.86	-70.08
W49N	19:10:13.335	+09:06:10	43.166	0.011	12.0	18.0	$35\farcs0 \times 35\farcs0$	19.65	$35\farcs0 \times 35\farcs0$	20.24	3.03
W51	19:23:44.0377	+14:30:29	49.489	-0.389	67.0	73.0	$35\farcs0 \times 35\farcs0$	1.98	$35\farcs0 \times 35\farcs0$	2.06	4.16

Table 5: Comparison of the 1.4 GHz continuum in the MeerKAT and JVLA HI spectral line observations.

Source					NE54-1420 MHz		VLA		
	R.A.	Dec	l	b	Beam	S_{cont}	Beam	S_{cont}	Diff
	[h:m:s]	[d:m:s]	[deg]	[deg]	[arcsec]	[Jy/b]	[arcsec]	[Jy/b]	[%]
W49N	19:10:14.9555	+09:06:17.9997	43.171	0.006	$35\farcs0 \times 35\farcs0$	5.38	$35\farcs0 \times 35\farcs0$	5.63	4.68
W51	19:23:42.385	+14:30:36.9997	49.487	-0.382	$35\farcs0 \times 35\farcs0$	7.86	$35\farcs0 \times 35\farcs0$	8.21	4.50

Table 6: Centroid velocity of selected OH 1665 MHz masers.

Source	NE54-1666		NE54-1667		(NE54-1667 – NE54-1666)	VLA		(VLA – NE54-1666)
	v_{cen}	dv_{cen}	v_{cen}	dv_{cen}	Δv_{cen}	v_{cen}	dv_{cen}	Δv_{cen}
	[km/s]	[km/s]	[km/s]	[km/s]	[km/s]	[km/s]	[km/s]	[km/s]
G09.622+0.19	1.479	0.002	1.478	0.004	-0.002	1.467	0.003	-0.013
NGC6334 I	-8.848	0.003	-8.858	0.011	-0.010	-8.851	0.004	-0.003
W49N	18.242	0.098	18.253	0.088	+0.011	18.261	0.065	+0.018
W51	55.974	0.017	55.980	0.041	+0.006	55.962	0.026	-0.012

center of all channels were about half a channel shifted with respect to each other, which made this an ideal test-case to check if the recovered flux of an unresolved spectral line is affected by the relative position of the maser peak with respect to the channel of the backend.

We observed four sources, NGC6334 I, G09.622+0.19, W49N and W51 for 10 min each in the NE54-1666 and NE54-1667 tunings, and for 5 min in NE54-1420 and NE54-1612. All of the sources were known to have strong masers in one of the OH main lines. We observed J1939-6342 as flux and bandpass calibrator at the beginning and at the end of the observations for 10 min (NE54-1666 and NE54-1667) and 5 min each (NE54-1420 and NE54-1612). We observed J1733-1304 and J2011-0644 between the target scans for complex gain calibration. For NE54-1666 and NE54-1667, we included a 5 min scan towards J1331+3030 (3C286) to be able to calibrate polarization.

We downloaded only selected channel ranges: Channels 15608 to 17655 to capture HI in NE54-1420, channels 14695 to 18540 and 14095 to 17940 to capture both OH main lines in NE54-1666 and NE54-1667, respectively, and channels 8192 to 24576 for NE54-1612, which actually encompasses the entire usable bandwidth for that setup. As recommended by S. Goedhart (priv. comm.), we deactivated automatic online flagging routines, as these potentially flag also strong maser lines, and applied only the following options during download: –static, –cam, –data_lost.

We used a calibration pipeline adapted for the MMGPS survey (S. Sridhar) with CASA version 6.2.1 (CASA Team et al. 2022; NE54-1612 was processed at a later point with version 6.5.2). As reference antennae we used m060. We derived the flux scale from J1939-6342 with the model of Steven-Reynolds 2016, and calibrated complex gains averaging both linear calibrations. To remove residual RFI from the calibration scans we applied automatic flagging (`tfcrop`). We note that the complex gain correction showed some variations towards J2011-0644, which may be due to some residual structure in this calibrator, which we did not correct for in this test. For NE54-1420, more detailed flagging was necessary: We flagged antennae m025, m031, m054, m056. We had to discard observations towards NGC6334 I and G09.622+0.19 as the initial part of the observations was corrupted. For this dataset we only used the final scan of J1939-6342 for bandpass calibration. Additionally, for NE54-1420 we determined the bandpass with polynomial fitting using the 'bpoly' option in `bandpass` after flagging channels with Galactic absorption in J1939-6342 – choosing a different bandpass calibrator for future HI observations may be advisable.

For comparison of the different MeerKAT observations, as well as the MeerKAT observations with ancillary VLA data, we reduced the data in two different ways: First, we reduced the MeerKAT data at native spectral ($\sim$0.3 km s^{-1}) and angular resolution (5″-20″). We set the Briggs weighting to robust=0 and used a pixel size of 1″. For imaging, we used the CASA task `tclean` (version 5.7.2 and 6.5.2). This data product was used for the comparison of strong OH 1665 MHz and OH 1667 MHz masers.

Second, to achieve a similar angular resolution as the JVLA observations for weaker 1612 MHz masers and, in the case of HI, for extended structures, we imaged the MeerKAT observations at lower resolution by selecting only visibilities in the range 0.5-10 kλ, and a uvtaper of 5″. We set the Briggs weighting to robust=0 and used a pixel size of 4″. We chose a fixed channel width of 0.6 km s^{-1}, which is twice the natural channel width of the MeerKAT observations. The correction and interpolation of the spectral axes to the local standard of rest were done automatically in `tclean`. Depending on size and available memory for data processing, we either imaged all channels together or divided then into smaller subsets and combined these afterwards to the final image cube.

We processed the JVLA observations (priv. comm.) similarly as above. First, at original angular resolution and with a fixed channel width of 0.2 km s^{-1}. Second, with a *uv*-taper of 10″ and not imposing limits on the uv-range of visibilities used for the cleaning. The JVLA observations were taken between July and September, 2021.

In the following, we focus on the brightest OH maser close to the center of the image in each transition/source. To compare the OH main line transitions of the two different MeerKAT tunings and the JVLA observations, we determined the peak pixel of the emission in the MeerKAT data, and extracted spectra towards the same coordinates in the VLA data. We estimated the continuum level from line-free channels and subtracted it for each spectrum individually. We note that while all datasets have slightly different angular resolutions, the maser sites are unresolved and appear as point sources in all datasets. Since OH 1665 MHz and OH 1667 MHz masers in star forming regions are typically very strong, we refrained from further smoothing the data to

prevent cleaning artifacts from being convolved into the spectra.

For the weaker OH 1612 MHz masers, as well as for the 1420 MHz transition, we compared all data on the same grid and with the same resolution. We smoothed all observations to a restoring beam of 35″ and gridded the MeerKAT observations on the JVLA observations.

Results: In the following, we compare both MeerKAT observations of the OH main lines in the MeerKAT NE54-1666 and NE54-1667 tunings. Then we compare MeerKAT with JVLA observations for all observable OH transitions and the HI line.

Comparison to MeerKAT observations at different tunings: Figure 1 shows the comparison of the OH main lines at 1665 MHz and 1667 MHz (Table 1) in the two MeerKAT observations NE54-1666 and NE54-1667. These tunings were shifted by 1 MHz. Due to different velocity corrections for the local standard of rest, for G09.622+0.19 and NGC6334 I, the different tunings resulted in channels shifted with respect to each other by half a channel. This allowed us to test if the flux of sometimes spectrally unresolved OH masers was still represented correctly irrespective of the tuning of the narrow band. For W49N and W51, the channels ended up being aligned in velocity for both observations, which served as reference sample. The observations were separated by 1 day.

The spectra from both observations are plotted on top of each other in Fig. 1. The spectra are displayed with their own spectral axes. The comparison was done on the integrated emission of selected maser spots. The integration range is indicated in blue dashed lines for each plot. The results are annotated in each panel, and summarized in Table 2, together with the position towards which the spectrum was extracted, as well as the angular resolution of the individual images.

We note the excellent agreement for both datasets in the OH 1667 MHz and OH 1665 MHz transition within a few percent. Two small outliers, which were still within 10%, are the OH 1667 MHz transitions for NGC6334 I (6%) and W49N (7%), which may have been due to slight differences during the cleaning process. The differences were comparable for G09.622+0.19 and NGC6334 I on the one hand, and W49N and W51 on the other hand. Since the two different tunings resulted in a shift of half a channel for the first group of sources, but in channel alignment for the second group, **we conclude that the OH maser fluxes in this test were not dependent on the tuning of the NE54**.

Comparison to previous JVLA observations: Comparing the OH main lines to ancillary JVLA observations revealed similar agreement as shown in Fig. 2. As indicated in Table 3, differences in the integrated emission of individual features amounted to ~10% for G09.622+0.19 and NGC 6334I, and for less than 3% for W49N and W51. We note that the restoring beams differed greatly for G09.622+0.19 and NGC 6334I, which may have been reason for the slightly larger differences in this case.

The OH 1612 MHz transition showed agreement better than <5% (Table 4; Fig. 3), with the exception for NGC6334 I, for which the flux of the VLA observations were 70% lower than the MeerKAT measurements. Unlike for the OH main lines discussed up to know, for this comparison we used the datasets which were reduced at the same angular resolution. To investigate the large difference in maser emission for NGC6334 I, we investigated a nearby source in Fig. 5. We found excellent agreement in continuum emission and in OH 1612 MHz line. We conclude that the increase in OH 1612 MHz emission was likely not an instrumental effect, but rather sign of maser variability, as has been seen in other maser transitions towards NGC6334 I (MacLeod et al. 2018).

In Fig. 4 we compared the HI absorption spectra for W49N and W51. The continuum values of the VLA and MeerKAT observations agreed within 5%. After normalizing both spectra, the absolute difference between JVLA and MeerKAT observations was better than 5σ in most channels, with deviations in certain velocity ranges for W51, which may have been due to differences in sensitivity to large-scale HI structure of MeerKAT and VLA.

To check the accuracy of the velocity scale, in Table 6 we compared the centroid velocities of the strongest OH 1665 MHz masers in each of the four sources. We interactively fitted Gaussian profiles using the CARTA viewer (Comrie et al. 2021; Cube Analysis and Rendering Tool for Astronomy) and reported the central velocity

of the Gaussian fit in Table 6, along with nominal fitting errors. We found that the peak velocities between different MeerKAT tunings and the ancillary JVLA observations agreed within nominal fitting errors. Differences appeared marginally larger than the formal errors for the difference between JVLA and MeerKAT observations for G09.622+0.19. This source, however, had an asymmetric line profile which indicated multiple components and may have affected the fits at the different channel widths of JVLA and MeerKAT observations.

Conclusion: Overall, we found that the MeerKAT NE54 correlator mode reproduces narrow spectral lines sufficiently well, irrespective of the channel alignment with the spectral line. We tested this on strong masers of the ground state hyperfine structure splitting transitions of OH at 18 cm. We compared different tunings of the MeerKAT NE54 correlator mode. A comparison with ancillary JVLA data revealed good agreement. This also holds for the HI 1420 MHz line. We found indications of an interesting variation of the 1612 MHz maser towards NGC6334 I, which is likely source-intrinsic rather than of instrumental origin, and which needs to be investigated with follow-up observations. A comparison of the velocity centroids of the OH 1665 MHz masers showed agreement between the spectral axes of the different MeerKAT tunings, as well as between MeerKAT and JVLA observations.

References

CASA Team, Bean, B., Bhatnagar, S., et al. 2022, PASP, 134, 114501

Comrie, A., Wang, K.-S., Hsu, S.-C., et al. 2021, CARTA: The Cube Analysis and Rendering Tool for Astronomy, Zenodo

Goedhart, S., van Rooyen, R., van der Walt, D. J., et al. 2019, MNRAS, 485, 4676

Jacob, A. M., Neufeld, D. A., Schilke, P., et al. 2022, ApJ, 930, 141

MacLeod, G. C., Smits, D. P., Goedhart, S., et al. 2018, MNRAS, 478, 1077

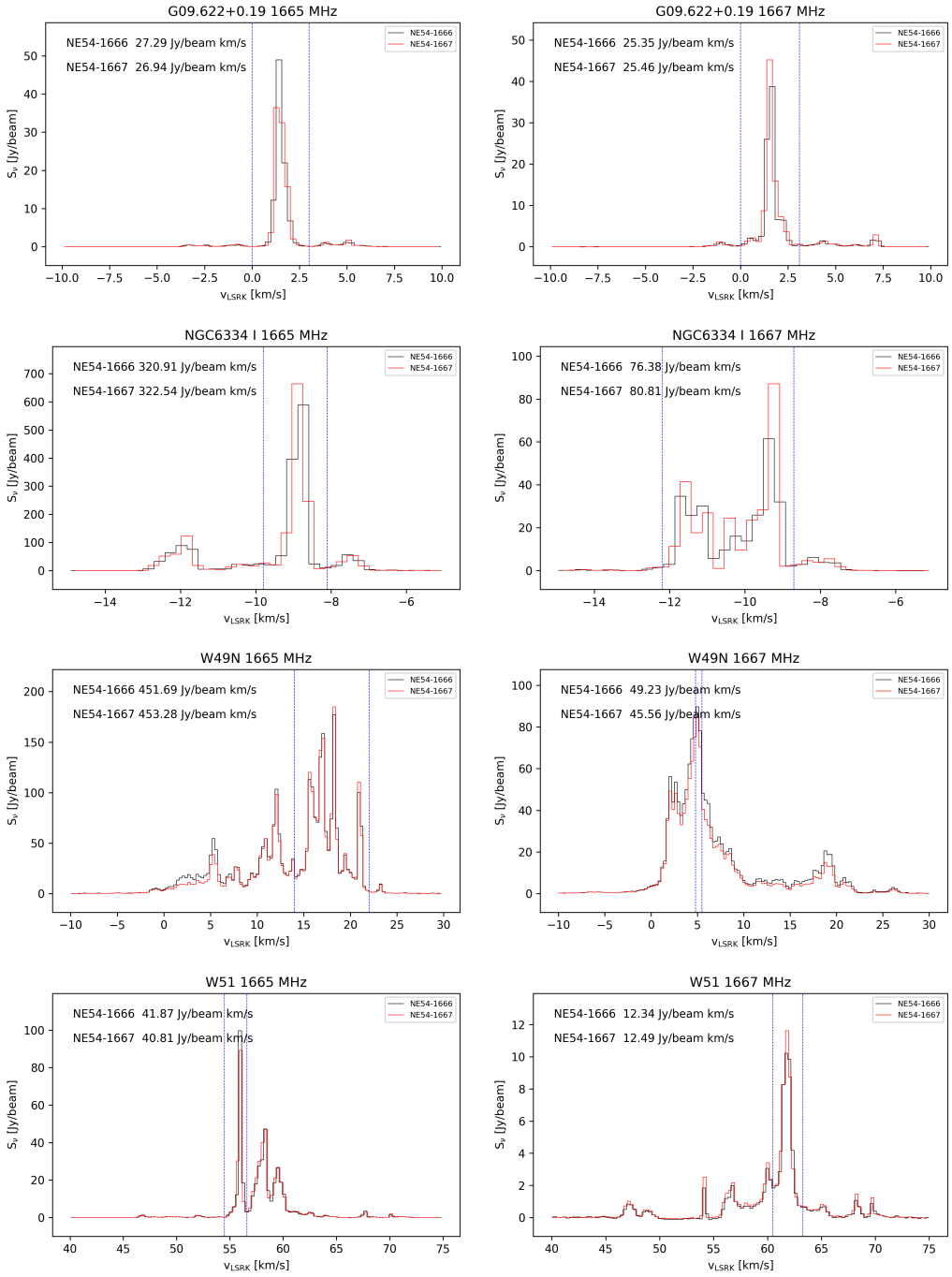

Figure 1: MeerKAT NE54-1666 vs. MeerKAT NE54-1667 for the OH 1665/1667 MHz transitions. Blue dashed lines indicate integration ranges, and the results annotated in the top left of the figure.

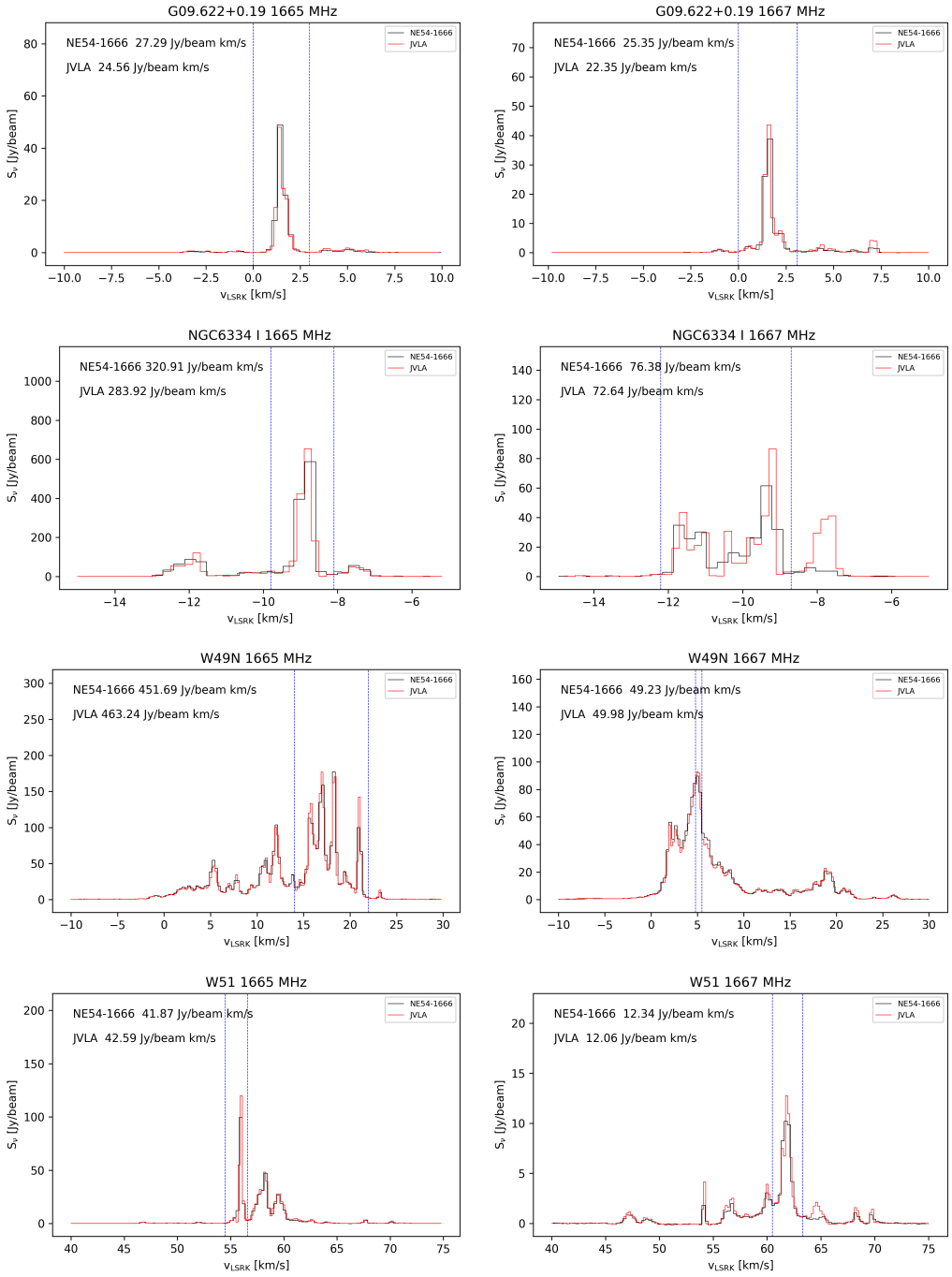

Figure 2: MeerKAT NE54-1666 vs. JVLA for the OH 1665/1667 MHz transitions. Lines and annotations as Fig. 1.

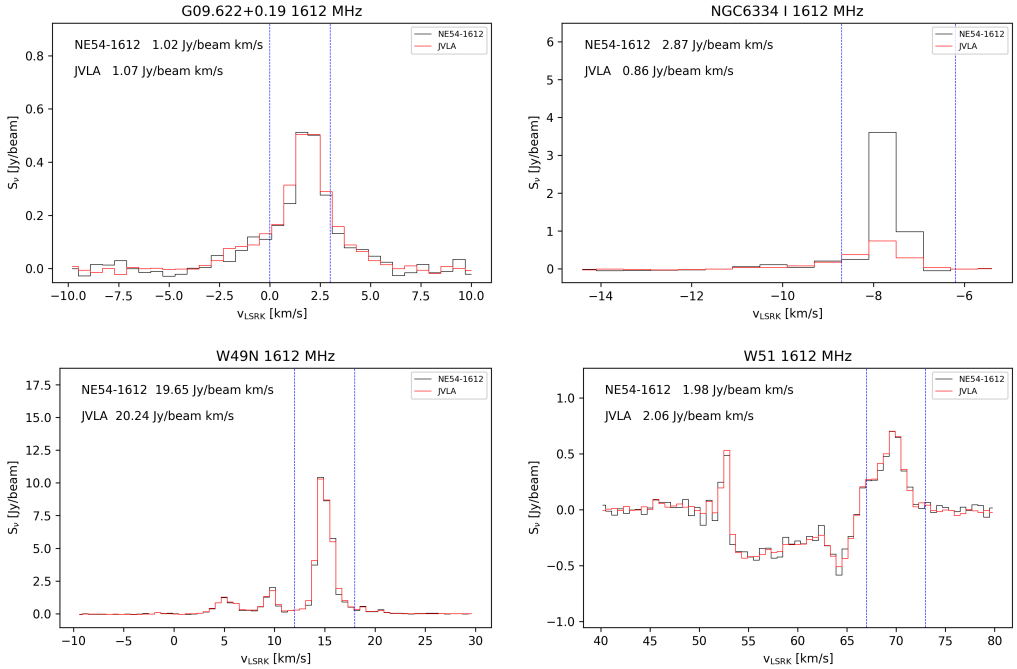

Figure 3: MeerKAT NE54-1612 vs. JVLA for the OH 1612 MHz transitions. Lines and annotations as Fig. 1.

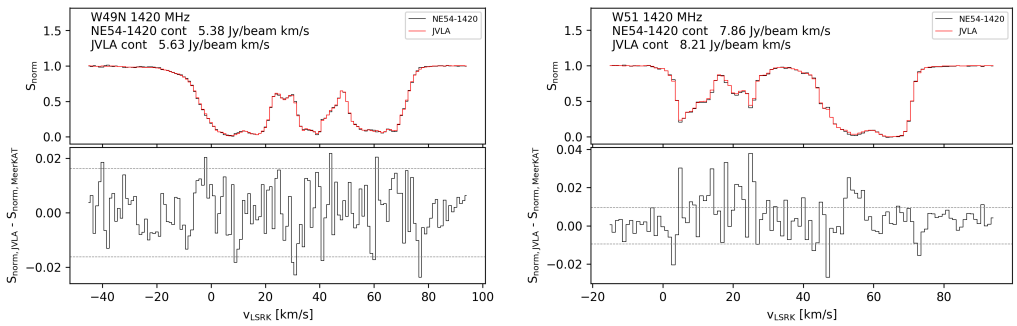

Figure 4: MeerKAT NE54-1420 vs. JVLA for the HI 1420 MHz transitions. The top panels show continuum-normalized spectra, with the continuum level indicated in the panel. The bottom panel shows the difference between the continuum-normalized spectra. Dashed lines indicate 3σ levels of the difference of the spectra.

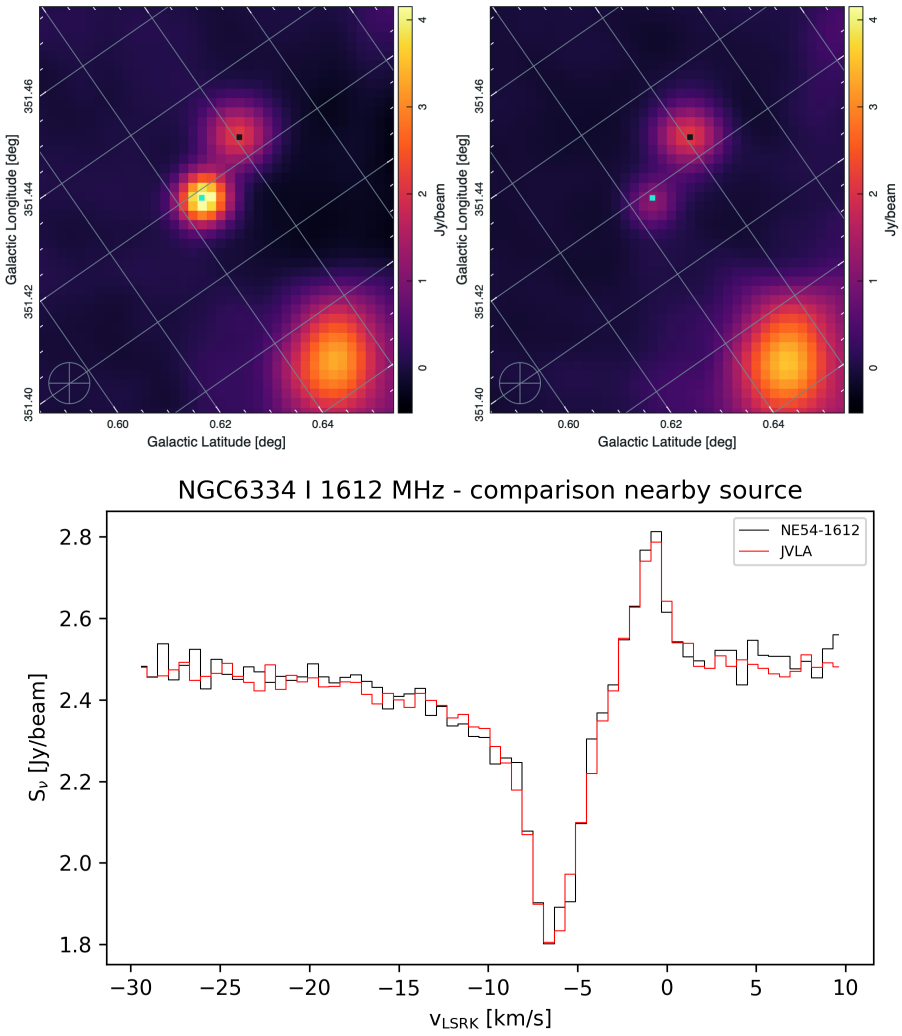

Figure 5: Comparison discrepancy MeerKAT vs. VLA for 1612 MHz maser in NGC6334 I. Channel images of the OH 1667 MHz transition at v=-7.8km s^{-1} from NE54-1666 and the VLA on the top left and top right, respectively. The dot in cyan marks the position of the 1612 MHz maser shown in Fig. 3. The black dot marks the position of a nearby continuum source, for which the spectra is shown in the bottom panel.